OFFICE OF NAVAL RESEARCH

GRANT or CONTRACT: N00014-91J-1201

R&T CODE: 4133032
Richard Carlin

TECHNICAL REPORT NO. 28

"Sol-gel-based Template Synthesis and Li-insertion Rate Performance of Nanostructured Vanadium Pentoxide"

by Charles J. Patrissi and Charles R. Martin

Prepared for Publication

in

Journal of the Electrochemical Society

Colorado State University
Department of Chemistry
Fort Collins, CO 80523-1872

June 1, 1999

REPORT DOCUMENTATION PAGE

1. June 1, 1999

2. Interim report

3. "Sol-gel-based Template Synthesis and Li-insertion Rate Performance of Nanostructured Vanadium Pentoxide"

4. GRANT: N00014-91J-1201, R&T CODE: 4133032

5. Charles J. Patrissi and Charles R. Martin

6. Charles R. Martin, Department of Chemistry, Colorado State University, Fort Collins, CO 80523-1872

7. TECHNICAL REPORT NO. 28

8. Office of Naval Research, Chemistry Division, 800 North Quincy Street, Arlington, VA 22217-5660

9. To be published in *Journal of the Electrochemical Society*

10. Reproduction in whole or in part is permitted for any purpose of the United States Government. This document has been approved for public release and sale; its distribution is unlimited.

11. Abstract: We have prepared nanostructured electrodes of orthohombic V_2O_5 using the template synthesis method. These electrodes were used to investigate the effects of Li-ion diffusion distance and surface area on V_2O_5 rate capability. Nanowires of V_2O_5 were prepared by depositing a precursor into the pores of microporous polycarbonate filtration membranes. This procedure yielded an ensemble of 115 nm diameter, 2 μm long nanowires of V_2O_5 which protruded from a V_2O_5 surface layer like the bristles of a brush. The galvanostatic discharge performance of these nanostructured V_2O_5 electrodes was compared to a thin film electrode of similar V_2O_5 mass and geometric area. The Li^+ storage capacity of the thin film electrode was equivalent to that of the nanostructured electrode at low (C/20) discharge rates. However, at a rate of 200C, the nanostructured electrode delivered three times the capacity of the thin film electrode. Above 500C the nanostructured electrode delivered four times the capacity of the thin film control electrode.

12. Subject terms: Nanostructured battery electrodes, V_2O_5, Li-ion batteries

17. 18. 19. Unclassified

Sol-gel-based Template Synthesis And Li-insertion Rate Performance Of Nanostructured Vanadium Pentoxide

Charles J. Patrissi* and Charles R. Martin**

Department of Chemistry, Colorado State University, Fort Collins, Colorado 80523, USA

ABSTRACT

We have prepared nanostructured electrodes of orthorhombic V_2O_5 using the template synthesis method. These electrodes were used to investigate the effects of Li-ion diffusion distance and surface area on V_2O_5 rate capability. Nanowires of V_2O_5 were prepared by depositing a precursor into the pores of microporous polycarbonate filtration membranes. This procedure yielded an ensemble of 115 nm diameter, 2 μm long nanowires of V_2O_5 which protruded from a V_2O_5 surface layer like the bristles of a brush. The galvanostatic discharge performance of these nanostructured V_2O_5 electrodes was compared to a thin film electrode of similar V_2O_5 mass and geometric area. The Li^+ storage capacity of the thin film electrode was equivalent to that of the nanostructured electrode at low (C/20) discharge rates. However, at a rate of 200C, the nanostructured electrode delivered three times the capacity of the thin film electrode. Above 500C the nanostructured electrode delivered four times the capacity of the thin film control electrode.

* Electrochemical Society Student Member.

** Electrochemical Society Active Member.

Introduction

The capacity of lithium-ion batteries at high discharge is critically dependent on the size and shape of the particles used to prepare the electrodes and on the morphology of the electrode material.[1-4] We have been investigating the effect of particle size and shape on electrode rate capability.[1,2] This is accomplished by using the template synthesis method[5,6] to prepare nanostructured electrode materials. These nanostructured electrodes consist of an ensemble of tubular or fibrillar particles of the electrode material which protrude from a current collector surface like the bristles of a brush. The template method allows for precise control of both the diameter and length of the tubules or fibrils that make up the nanostructured electrodes. To date we have explored the rate capabilities of nanostructured TiS_2[1] and $LiMn_2O_4$[2] electrodes prepared via the template-synthesis method.

In these prior investigations, the rate capabilities of the nanostructured electrodes were compared with the rate capabilities of thin-film electrodes containing the same type and quantity of the electrode material. Galvanostatic discharge experiments showed that the nanostructured electrodes delivered higher capacities, at high discharge currents, than the thin film electrodes. This is because, for the nanostructured electrode, the Li^+ diffusion distances are shorter and the surface areas are higher. Diffusion distance and surface area dramatically affect rate capability because Li^+ diffusion within the electrode material is slow.[7] At high discharge rate, high Li^+ insertion-flux density and slow Li^+ transport result in concentration polarization of Li^+ within the electrode material. This causes a drop in cell voltage which results in termination of the discharge before the maximum capacity of

the electrode material is utilized.[8] Decreasing the average diffusion distance, while keeping the mass constant, increases the surface area of the electrode and lowers current density. This results in the delay of concentration polarization to higher current values and, consequently, increased electrode rate capability.

Sol-gel chemistry is a simple and efficient route for preparing inorganic compounds such as glasses and ceramics.[9] Recently we combined sol-gel chemistry and template synthesis to prepare micro- and nanostructures of inorganic oxides such as TiO_2, WO_3 and ZnO.[10] In this paper we report the use of a sol-gel template method to prepare nanostructured electrodes of crystalline V_2O_5. Galvanostatic experiments were used to explore the rate capabilities of the nanostructured electrodes relative to thin-film control electrodes of the same material. We show here that the Li^+ storage capacities of the nanostructured and thin-film electrodes are equivalent at slow discharge rates (C/20). However, the capacity of the nanostructured electrode is 4 times higher at discharge rates above 500C.

Experimental

Template Synthesis of the V_2O_5 Nanofibers. Template synthesis is a general method for preparing nanomaterials and is described in detail elsewhere.[5,6] Briefly, template synthesis entails deposition of the material of interest, or a precursor for that material, into the pores of a microporous template membrane. The templates used here were polycarbonate filtration membranes (Poretics, Inc.) with a nominal pore diameter of 50 nm. The pores are cylindrical, nearly monodisperse in diameter and extend through the thickness (6 μm) of the template membrane.

It is well known that crystalline V_2O_5 and other vanadium oxides can be prepared by the sol-gel route via hydrolysis and condensation of alkoxide precursors.[11] Sol-gel chemistry and template synthesis were combined to prepare the nanostructured crystalline V_2O_5 electrodes. Figure 1 shows a schematic of this template synthesis procedure. A 1.5 cm^2 section of template membrane was placed on a Pt current collector (1.5 x 3 cm) in a glove box purged with argon. Next, a microliter syringe was used to apply 0.6 μL of the V_2O_5 precursor, triisopropoxyvanadium (V) oxide (TIVO) (Strem Chemical, > 98%) to the template membrane surface. The TIVO filled the pores in the template membrane and the space between the membrane and the underlying Pt current collector.

Hydrolysis of TIVO in air is extremely fast and this resulted in cracking of the nascent V_2O_5 nanofibers forming within the template membrane. In order to prevent this, hydrolysis of the precursor was carried out in a glove box under very low water partial pressures. The reaction was allowed to proceed for 12 hours which resulted in the formation of nanofibers of a TIVO gel. After gel formation, the composite was removed from the glove box and heated in air at 80 °C for 2 hours. The template membrane was then removed with an oxygen plasma (15 watts rf power, 100 mTorr O_2, 2 hours). Finally, dehydration and condensation of the precursor to crystalline V_2O_5 was accomplished by heating at 400 °C for 10 hours in 150 psi O_2.

Preparation of the Thin Film Control Electrodes. Thin film control electrodes were prepared by depositing liquid TIVO onto a Pt foil current collector. This was done as above using a glass micropipette to spread the precursor evenly over the Pt foil surface. Again, hydrolysis proceeded for 12 hours in the glove box after which time the liquid had hydrolyzed to a yellow film of TIVO gel. In order to make the geometric area of the thin

film control electrode approximately equal to that of the nanostructured electrode, all but 1.4 cm^2 of the TIVO gel film was removed with a water-wet cotton swab. The TIVO gel/Pt composite was then thermally treated in the same way as the nanostructured electrode.

Characterization. V_2O_5 morphology and crystallinity were investigated with a Phillips 505 scanning electron microscope and a Phillips powder X-ray diffractometer (Cu Kα). V_2O_5 mass was determined after all electrochemical experiments were completed by immersing the electrode in 2M H_2SO_4, followed by analysis for vanadium content with a Perkin Elmer Plasma 400 atomic emission spectrometer.

Chronopotentiometry and cyclic voltammetry were performed under argon using a three electrode cell. Li foil counter and reference electrodes were used. The electrolyte was 1M $LiClO_4$ in a 7:3 (v/v) mixture of diethyl carbonate (99%, Aldrich) and ethylene carbonate (battery grade, Ferro Corp.); both solvents were used as received. Chronopotentiometric data was acquired using an EG&G model 263A potentiostat/galvanostat and model 270/250 research electrochemistry software. Cyclic voltammetry was performed with a Bioanalytical Systems CV-27 voltammograph between the voltage limits 3.80 and 2.50 V (vs. Li/Li^+).

Results and Discussion

Morphology and Crystallinity. Figure 2 shows scanning electron micrographs of a typical nanostructured V_2O_5 electrode. Figure 2A is a lower magnification image that shows the V_2O_5 fibrils dispersed across the surface of this nanostructured electrode. Figure 2B is a higher magnification image that was used to determine the average length and diameter of

the V_2O_5 nanofibrils. The average length was 2 ± 0.25 μm and the average diameter was 115 ± 14 nm. This diameter is more than the nominal diameter of the pores in the template (50 nm as reported by the manufacturer). Such larger-than-expected nanofibril diameters have been observed previously with these polycarbonate template membranes.[12,13] Two explanations have been proposed – that the pore expands during formation of the nanofibril[13] and that the pore diameter is smaller at the surface of the membrane than in the middle[12].

As noted above, the V_2O_5 nanofibrils protrude from a V_2O_5 surface film. This surface film results because the TIVO precursor fills the space between the membrane and the Pt current collector surface. An SEM image of this surface layer is shown in Figure 2C. The fibrils that had been attached to this section of the surface layer were removed by lightly brushing with a dry cotton swab. The surface layer is continuous and relatively smooth. Images like that shown in Figure 2C were used to obtain the average thickness of the V_2O_5 surface layer. An average thickness of 97 ± 20 nm was obtained.

The length and diameter of the fibrils along with the average thickness of the surface layer allow for a calculation of the relative volumes of the V_2O_5 nanofibrils and the V_2O_5 surface layer. This calculation showed that the volume of the nanofibrils is 1.25 times the volume of the surface layer. This is important because during the charge/discharge experiments (see below) Li^+ intercalates into both the fibrils and the surface film. Li^+ that intercalates into the fibrils must diffuse approximately 57 nm (the radius of the fibrils), whereas Li^+ that intercalates into the surface film must diffuse approximately 97 nm (the thickness of the film). As we will see below, both of these diffusion distances are small relative to the corresponding distance in the thin film control electrode (Table I).

The thin-film control electrodes represent a more conventional electrode configuration, for example like those developed for thin-film lithium micro-batteries.[14-16] An SEM image of the thickness of such an electrode is shown in Figure 3. This image was obtained by bending the underlying Pt foil current collector to 180° and examining the fractured film edge. Images of this type have shown that the thin-film control electrodes are 250 ± 30 nm in thickness. In addition to SEM, profilometry was used to confirm that the film thickness was ≈ 250 nm.

Table I shows the important physical characteristics of the electrodes used in this study. The surface area of the thin-film control electrode was calculated from the geometric area of 1.4 cm^2 (1.0 cm x 1.4 cm) and the known mass of the film. The calculation of the surface area of the nanofibril electrode was based on an average fibril length of 2 μm, a fibril density of $6x10^8$ fibrils cm^{-2}, an average fibril diameter of 115 nm, and the geometric area of the membrane used, 1.5 cm^2. As shown in Table I, the nanostructured electrodes have both higher surface area and shorter Li^+ diffusion distances than the thin-film control electrode. As will be shown below, both of these features allow for greater rate capabilities for the nanostructured electrode.

Powder X-ray diffraction (XRD) patterns for the thin-film control and nanostructured electrodes are shown in Figure 4A and 4B, respectively. The expected powder pattern for orthorhombic V_2O_5 is shown in Figure 4C for comparison.[17] Note that the intensity ratios of the peaks for both the nanostructured and the thin-film V_2O_5 do not correspond exactly to the expected pattern for orthorhombic V_2O_5. The larger than expected 001 peaks in Figure 4A and 4B indicate that a majority of the crystallites are oriented with their "a" and "b" axes parallel to the surface of the Pt current collector. This preferred orientation is

especially pronounced for the thin-film V_2O_5 electrode where the 001 peak is observed almost exclusively (Figure 4A). Similar results have been reported previously for V_2O_5 thin films prepared from alkoxides.[18] The starred peaks in Figure 4B are due to impurities within the sample chamber.

Electrochemistry. The charge and discharge reactions for V_2O_5 can be written as follows:

$$xLi^+ + xe^- + V_2O_5 \underset{\text{charge}}{\overset{\text{discharge}}{\rightleftharpoons}} Li_xV_2O_5 \qquad (1)$$

GITT[19] and open-circuit voltage[20] experiments have shown that when a cutoff voltage of 2.50 vs. Li/Li^+ is used, the maximum value of x in Equation 1 for orthorhombic V_2O_5 is x = 1. This corresponds to a capacity of 147 mAh g^{-1} V_2O_5. This was confirmed for our electrodes by measuring the discharge capacities for five nanostructured electrodes and three thin-film electrodes at discharge rates between C/19 and C/23. The means and standard deviations of these results were $x = 1.05 \pm 0.04$ for the nanofibrillar electrodes and $x = 1.01 \pm 0.05$ for the thin film controls.

Figure 5 shows constant current charge and discharge curves for the nanofibrillar electrode (Figure 5A) and the thin-film electrode (Figure 5B) at discharge and charge rates of C/20. The shapes of the discharge curves are similar to those reported previously for Li^+-intercalation into orthorhombic V_2O_5 at low discharge and charge rates.[19-21] For the electrochemical cell used here, cell voltage is related to the chemical potential of Li in V_2O_5 by

$$E = (\mu_o - \mu)/F \qquad (2)$$

where E is the measured cell voltage, μ_o and μ are the chemical potentials of lithium at the surfaces of the reference electrode and V_2O_5, respectively, and F is Faraday's constant.[8] According to Equation 2, the areas of sloping cell voltage in Figure 4 are caused by a change in Li chemical potential with quantity of Li^+ intercalated. Previous reports[19,20] show that these regions of sloping voltage correspond to $Li_xV_2O_5$ compositions where only a single crystalline phase exists. Therefore, μ and cell voltage change with the activity of Li in the V_2O_5. The plateaus are compositions where two crystalline phases co-exist in equilibrium. Because of the two-phase equilibrium, μ and cell voltage are independent of composition.

In order to completely characterize the rate capabilities of these various electrodes, 15 complete charge and discharge cycles, at various rates, were conducted on each electrode. We were concerned that the capacity of the electrode might fade during these 15 charge/discharge cycles.[22] This would make interpretation of the dependence of capacity on discharge rate (Figure 8) more difficult. However, we found that the capacity of the first and fifteenth discharge (at low discharge rate) were the same within experimental error.

To further explore this issue of capacity fade, cyclic voltammetric experiments were done on a second set of nanostructured and thin-film electrodes. These electrodes were cycled at a scan rate of 1.00 mV s^{-1} between the limits of 3.80 V and 2.50 V. After each scan, the potential was held at 3.80 V until the current decayed to the first scan value. The data obtained are shown in Figure 6. After 40 complete discharge/charge cycles, the nanostructured electrode had 93% of its initial (first-cycle) capacity. The thin-film electrode retained 89% of its initial capacity.

Electrode rate capability was studied by following discharge capacity with increasing discharge rate, Figure 7. Figure 7 shows electrode capacity vs. cell voltage at various discharge rates for the nanostructured electrode (7A) and the thin-film control electrode (7B). The current densities used for the nanostructured electrode were from 0.47 $\mu A\ cm^{-2}$ (C/20) to 13.3 $mA\ cm^{-2}$ (1361C) and for the thin-film electrode were from 0.48 $\mu A\ cm^{-2}$ (C/20) to 11.4 $mA\ cm^{-2}$ (1190C). Both the nanofibrillar and thin-film control electrodes show the experimental maximum capacity of $x = 1$ at low discharge rates (C/20). However, Figure 7 also shows that increasing the discharge rate reduces the degree of lithium insertion and thus the discharge capacity of the electrodes. In general, the data show that the discharge capacity of the nanostructured electrode remains higher, at high discharge rate, than the discharge capacity of the thin-film electrode. As has been discussed in our previous work,[1,2] this is due to the shorter Li^+ diffusion distance and higher surface area (Table I) of the fibrillar material relative to the thin-film control. Higher surface area is important because it lowers Li^+-insertion rate density during the discharge process. This lower insertion rate delays the capacity loss associated with concentration polarization to higher discharge currents.

In order to conduct multiple experiments, the electrodes were "recharged" after each discharge experiment. This was accomplished using a positive voltammetric scan from the open circuit potential to 3.80 V (vs. Li) at a sweep rate of 0.20 $mV\ s^{-1}$. The electrode was held at this potential until the current decreased to the first scan value. In all experiments the anodic capacity measured during the voltammetric sweep was equivalent to the discharge capacity. This shows that the discharge capacity was 100% faradaic.

A more direct comparison of the rate capability of the nanostructured and thin-film electrodes is shown in Figure 8. The data points shown in this figure were obtained from the discharge capacity values shown in Figure 7 at a voltage cutoff of 2.50 V. The capacity of the nanofibrillar electrode is approximately 3 times higher at a discharge rate of 200C and increases to 4 times higher at discharge rates between 500 and 1190C. Figure 8, then, clearly shows the rate capability advantages of the nanostructured electrode due to higher surface area and smaller diffusion distances.

Conclusion

We have demonstrated a simple and efficient template synthesis method for the preparation of nanofibrillar, orthorhombic V_2O_5 electrodes. Investigation of the rate capabilities of these electrodes show, as per our previous work,[1,2] that the nanofibrillar electrodes can deliver higher capacities, at high discharge currents, relative to a thin-film control electrode.

The ultimate goal for battery and electrode performance is high energy output at both low and high power. At low power (22 mW g^{-1} V_2O_5), the nanostructured electrode shown here delivered the expected maximum specific energy of approximately 467 mWh g^{-1} V_2O_5. These values were calculated from the results of a constant current experiment where the discharge rate was C/21 (700 nA), the mean discharge voltage was 3.167 V, the electrode capacity was $Li_{1.0}V_2O_5$ and the cutoff voltage was 2.500 vs. Li/Li^+. At extremely high power (534 W g^{-1} V_2O_5) the energy output was 85 mWh g^{-1} V_2O_5. The discharge rate for this experiment was 1361C (20 mA) and the mean discharge voltage was 2.662 V. These results show that the nanostructured V_2O_5 is capable of useful specific energy even at extremely high specific power.

In addition to useful specific energy at high specific power, a practical battery electrode must also have high volumetric energy density. From this point of view, the electrodes prepared here must be viewed as experimental systems meant to explore the specific power capabilities of the nanostructured electrode concept. This is because these nanostructured electrodes were prepared from template membranes with low porosity and, therefore, low fibril density. It is important to point out, however, that nanostructured electrodes with 30 to 50 times higher volumetric energy density could be prepared using template membranes with higher porosity. For example, the templates used for this fundamental study contain a total pore volume that is approximately 1.2% of the volume of the membrane. We have prepared template membranes in our lab with porosities as high as 30%.[23] In addition, templates have been reported in the literature with porosities of approximately 50%.[24] We are currently using such high porosity templates to prepare nanostructured V_2O_5 electrodes.

Acknowledgement

We thank the United States Department of Energy, the Office of Naval Research and the Link Foundation for financial support.

References

1. Che, G.; Jirage, K. B.; Fisher, E. R.; Martin, C. R., *J. Electrochem. Soc.*, **144**, 4296 (1997).

2. Nishizawa, M.; Mukai, K.; Kuwabata, S.; Martin, C. R.; Yoneyama, H., *J. Electrochem. Soc.*, **6**, 1923 (1997).

3. Tipton, A. L.; Passerini, S.; Owens, B. B.; Smyrl, W. H., *J. Electrochem. Soc.*, **143**, 3473 (1996).

4. Tran, T. D.; Feikert, J. H.; Pekala, R. W.; Kinoshita, K., *J. Appl. Electrochem.*, **26**, 1161 (1996).

5. Martin, C. R., *Science*, **266**, 1961 (1994).

6. Martin, C. R., *Accounts of Chemical Research*, **28**, 61 (1995).

7. Scrosati, B., *J. Electrochem. Soc.*, **139**, 2776 (1992).

8. Owen, J. R., *Chem. Soc. Rev.*, **26**, 259 (1997).

9. Livage, J.; Henry, M.; Sanchez, C., *Prog. Solid St. Chem.*, **18**, 259 (1988).

10. Lakshmi, B. B.; Dorhout, P. K.; Martin, C. R., *Chem. Mater.*, **9**, 857 (1997).

11. Nabavi, M.; Sanchez, C.; Livage, J., *Eur. J. Solid State Inorg. Chem.*, **28**, 1173 (1991).

12. Schonenberger, C.; Zande, B. M. I. v. d.; Fokkink, L. G. J.; Henny, M.; Schmid, C.; Kruger, M.; Bachtold, A.; Huber, R.; Birk, H.; Staufer, U., *J. Phys. Chem. B*, **101**, 5497 (1997).

13. Wang, L.; Yu-Zhang, K.; Metrot, A.; Bonhomme, P.; Troyon, M., *Thin Solid Films*, **288**, 86 (1996).

14. Liu, P.; Zhang, J.-G.; Turner, J. A.; Tracy, C. E.; Benson, D. K.; Bhattacharya, R. N., *Solid State Ionics*, **111**, 145 (1998).

15. Jones, S. D.; Akridge, J. R., *Solid State Ionics*, **86-88**, 1291 (1996).

16. Bates, J. B.; Gruzalski, G. R.; Dudney, N. J.; Luck, C. F.; Yu, X.-H.; Jones, S. D., *Solid State Technology*, **36**, 59 (1993).

17. *X-ray Powder Data File*; American Society for Testing and Materials.: Philadelphia, 1962; Vol. card# 9-387.

18. Livage, J., *Chem. Mater.*, **3**, 578 (1991).

19. Delmas, C.; Cognac-Auradou, H.; Cocciantelli, J. M.; Menetrier, M.; Doumerc, J. P., *Solid State Ionics*, **69**, 257 (1994).

20. Dickens, P. G.; French, S. J.; Hight, A. T.; Pye, M. F., *Mat. Res. Bull.*, **14**, 1295 (1979).

21. Vivier, V.; Farcy, J.; Pereira-Ramos, J.-P., *Electrochimica Acta*, **44**, 831 (1998).

22. Bates, J. B.; Gruzalski, G. R.; Dudney, N. J.; Luck, C. F.; Yu, X., *Solid State Ionics*, **70/71**, 619 (1994).

23. C.A. Foss, J.; Hornyak, G. L.; Stockert, J. A.; Martin, C. R., *J. Phys. Chem.*, **98**, 2963 (1994).

24. Masuda, H.; Fukuda, K., *Science*, **268**, 1466 (1995).

Figure Captions

Figure 1. Schematic of template synthesis method used to prepare the nanostructured V_2O_5 electrodes. The V_2O_5 precursor was triisopropoxyvanadium (V) oxide, VTIPO. Polycarbonate microporous filtration membranes were used as templates.

Figure 2. SEM images of the components of a nanostructured electrode. **A.** Low magnification image of the V_2O_5 nanofibrils. **B.** High magnification image of the nanofibrils. **C.** The underlying V_2O_5 surface layer .

Figure 3. SEM image of an edge view of a typical V_2O_5 thin-film control electrode.

Figure 4. Powder X-ray diffraction pattern for thin film (A) and nanostructured (B) V_2O_5 electrodes on Pt. The vertical lines (C) show the XRD pattern for orthorhombic V_2O_5 as given in ref. 17.

Figure 5. Galvanostatic discharge and charge curves for nanostructured (A) and thin film (B) V_2O_5 electrodes at C/20.

Figure 6. Electrode discharge capacity as a function of cycle number. Data was obtained via cyclic voltammetry as explained in the text.

Figure 7. Cell voltage vs. capacity for nanostructured (7A) and thin-film (7B) electrodes at various discharge rates. $Li_{1.0}V_2O_5$ is equivalent to a discharge capacity of 147 mAh g^{-1}.

Figure 8. Discharge capacity of typical nanostructured and thin film electrodes as a function of galvanostatic discharge rate.

Table I. Characteristics of the Nanostructured and Thin-Film Control Electrodes.

Electrode	V_2O_5 Mass (μg)	V_2O_5 Surface Area ($m^2\ g^{-1}$)	Li^+ Diffusion Distance
Nanostructured	99.7	8.0	Surface Layer ≈ 100 nm Nanofibrils ≈ 57 nm
Thin Film	92.0	1.5	≈ 250 nm

Figure 1

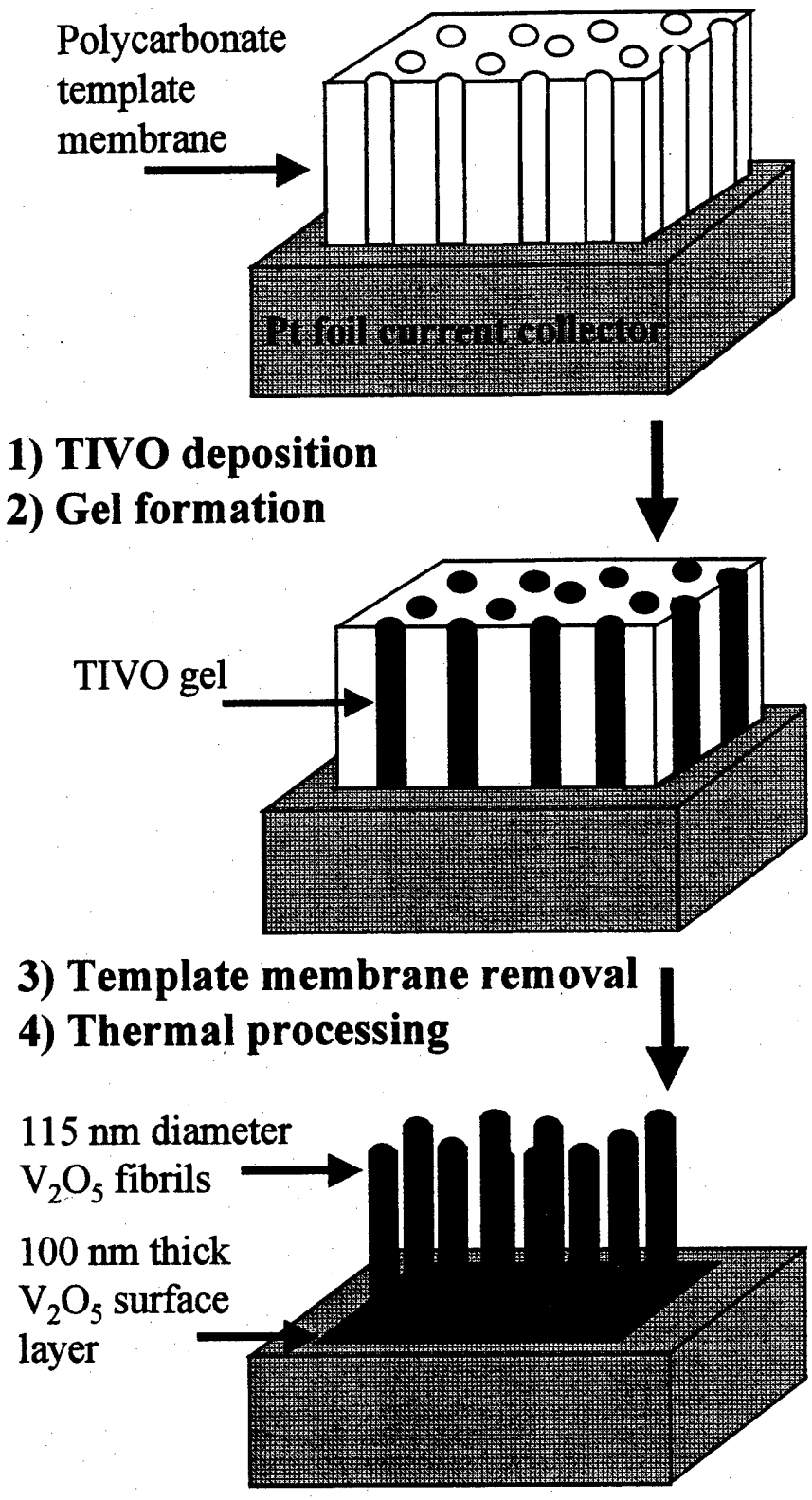
Polycarbonate template membrane
Pt foil current collector
1) TIVO deposition
2) Gel formation
TIVO gel
3) Template membrane removal
4) Thermal processing
115 nm diameter V_2O_5 fibrils
100 nm thick V_2O_5 surface layer

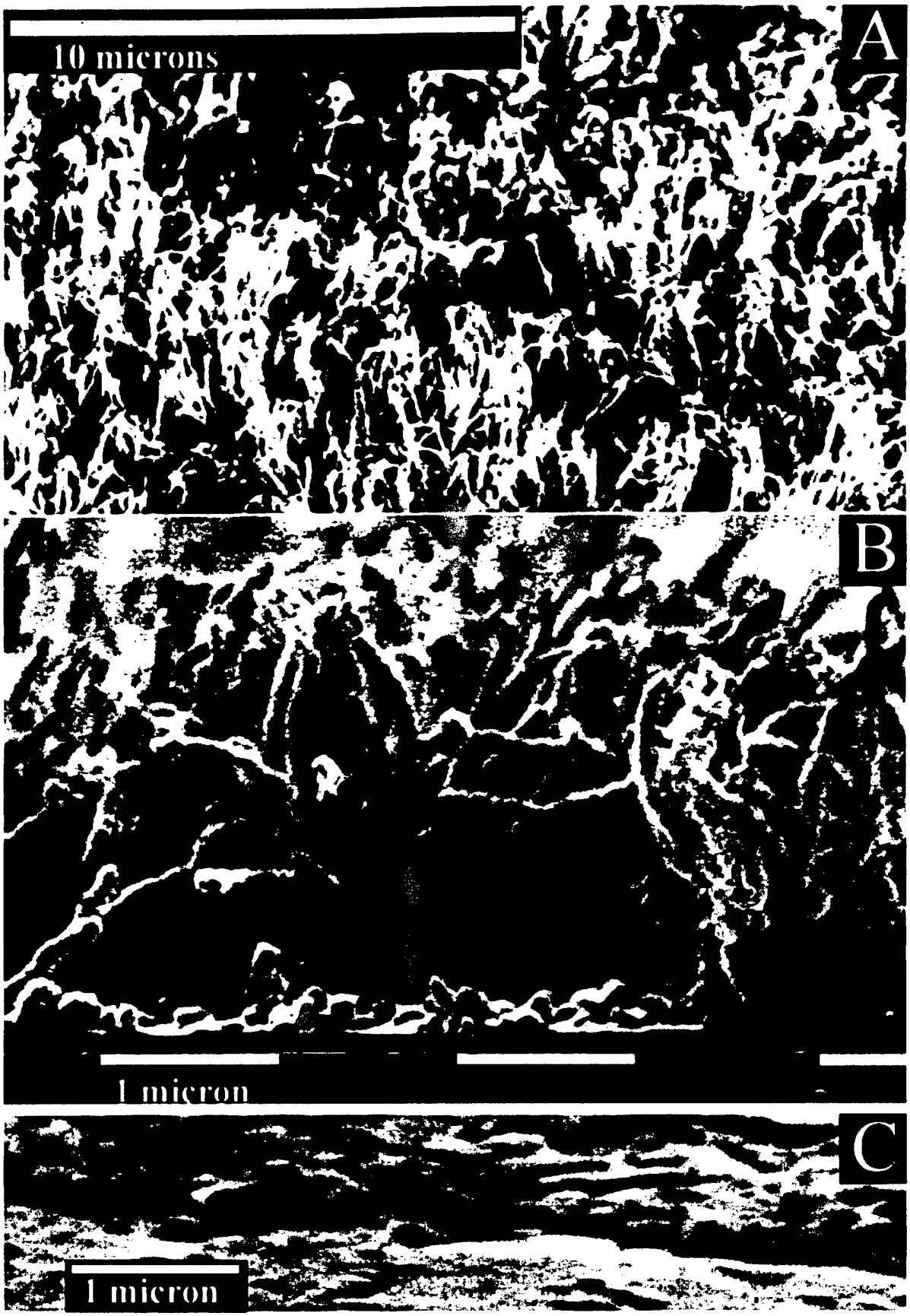
10 microns
A
B
1 micron
C
1 micron


1 micron

Figure 4

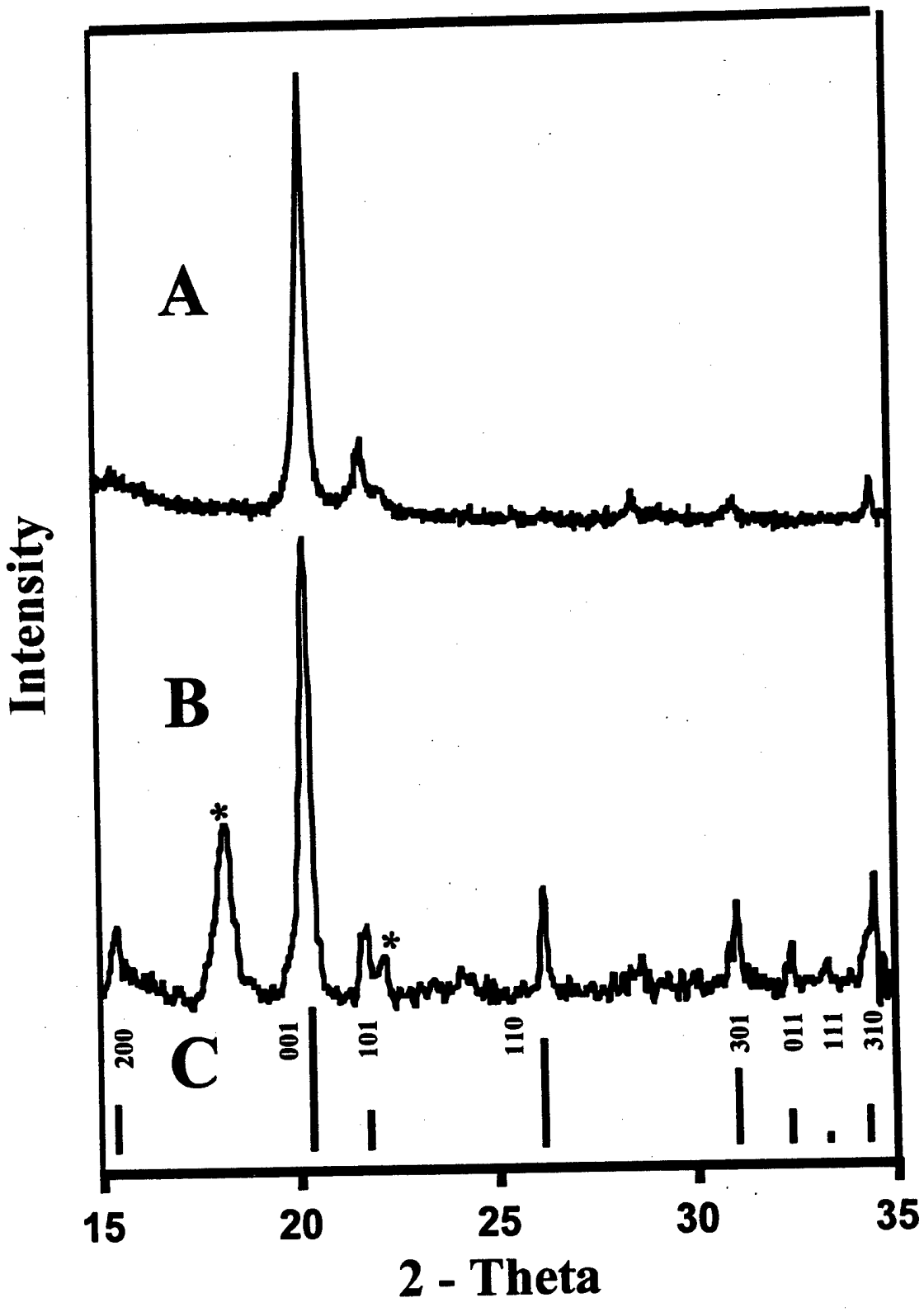
A
B
C
Intensity
200
001
101
110
301
011
111
310
*
*
15
20
25
30
35
2 - Theta

Figure 5

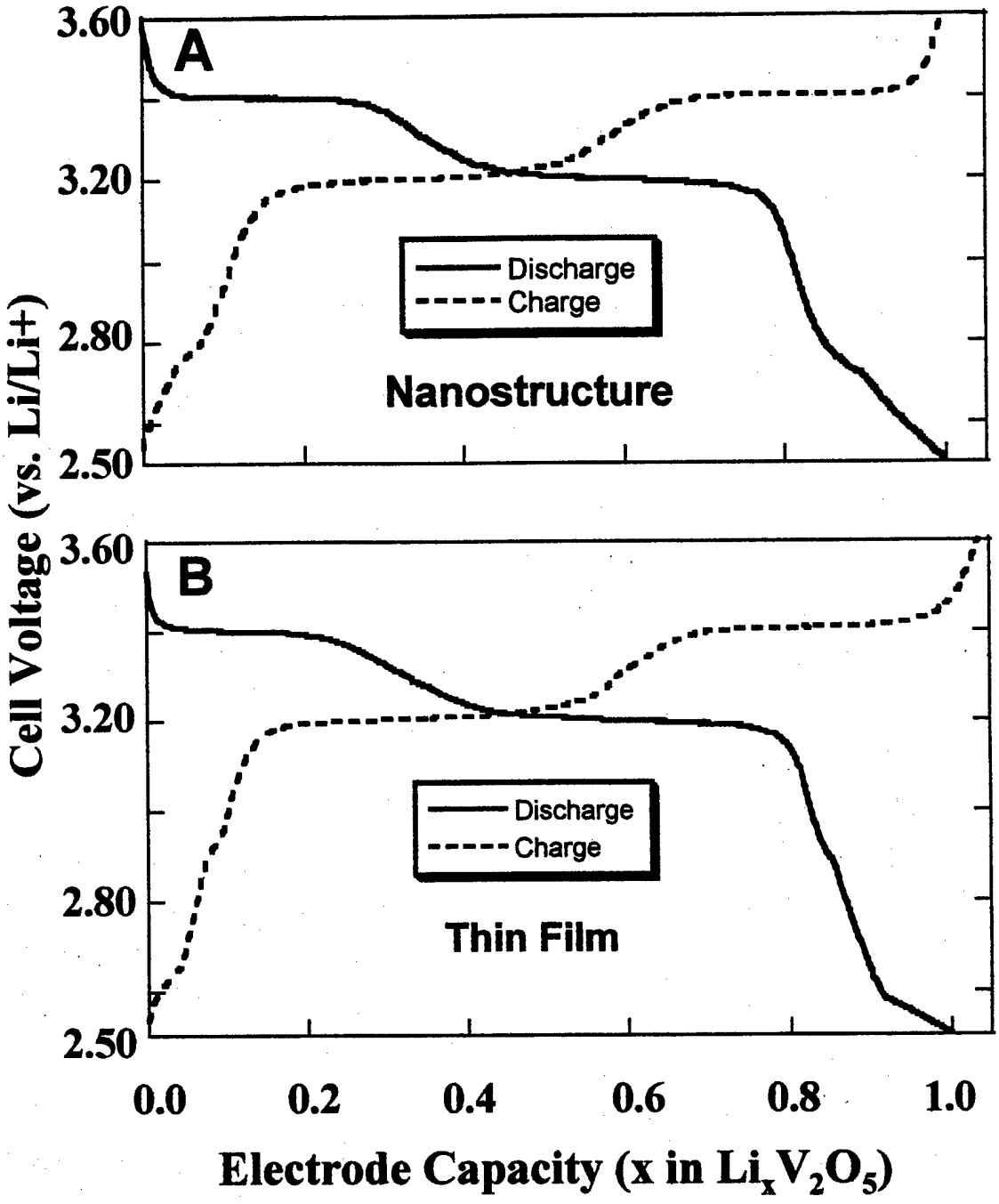
A
B
3.60
3.20
2.80
2.50
Discharge
Charge
Nanostructure
Thin Film
Cell Voltage (vs. Li/Li+)
0.0
0.2
0.4
0.6
0.8
1.0
Electrode Capacity (x in $Li_xV_2O_5$)

Figure 6

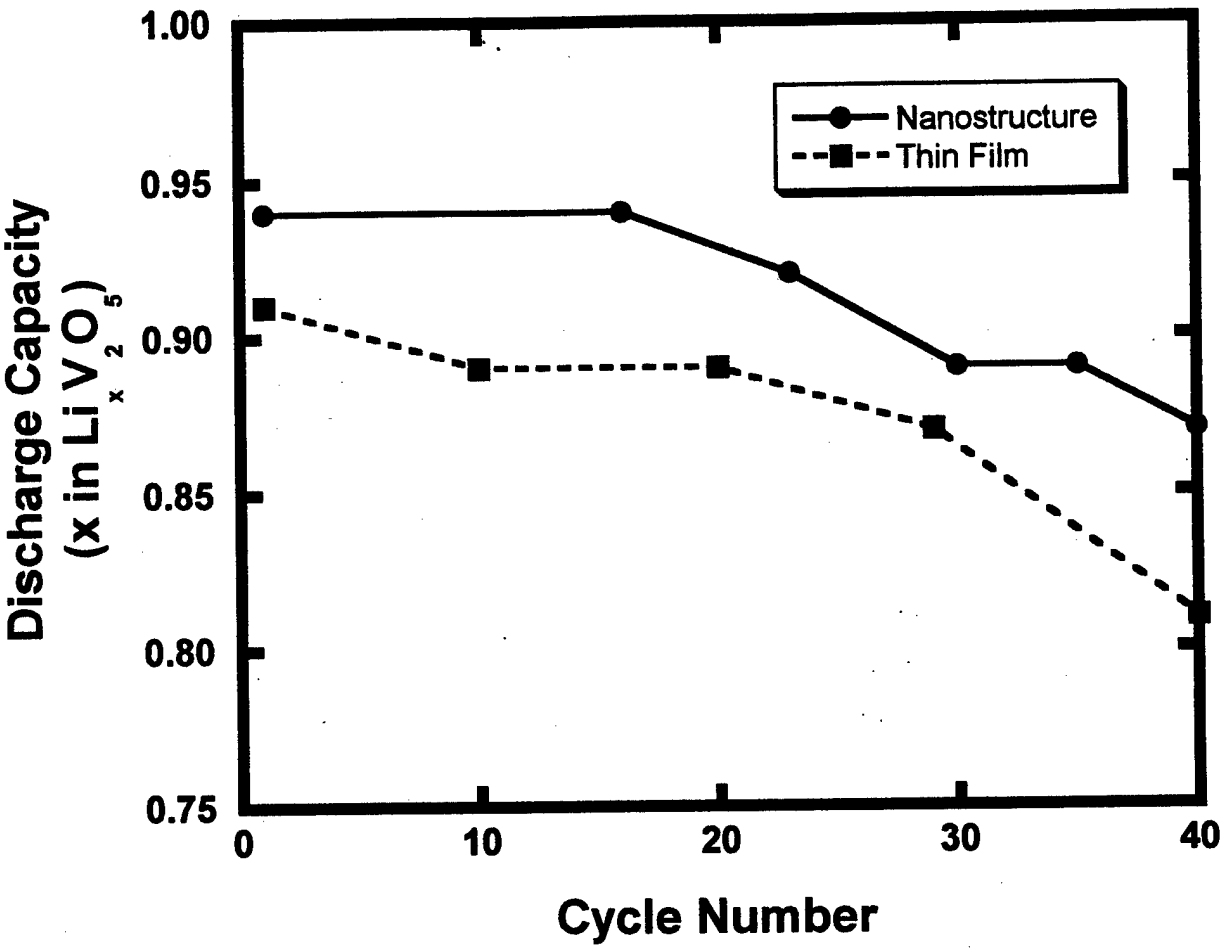
1.00
0.95
0.90
0.85
0.80
0.75
0
10
20
30
40
Discharge Capacity
(x in Li V O)
x 2 5
Cycle Number
Nanostructure
Thin Film

Figure 7

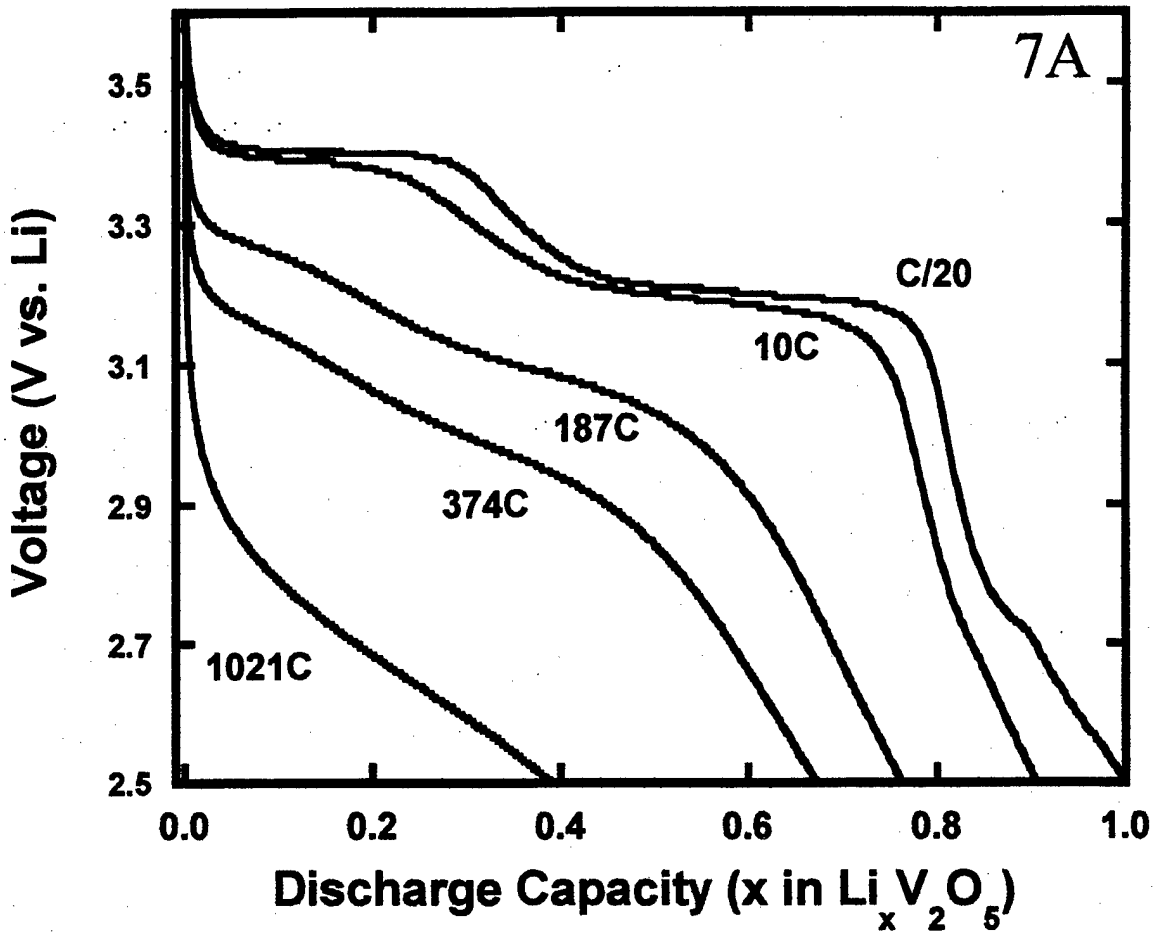
7A
Voltage (V vs. Li)
3.5
3.3
3.1
2.9
2.7
2.5
C/20
10C
187C
374C
1021C
0.0
0.2
0.4
0.6
0.8
1.0
Discharge Capacity (x in Li$_x$V$_2$O$_5$)

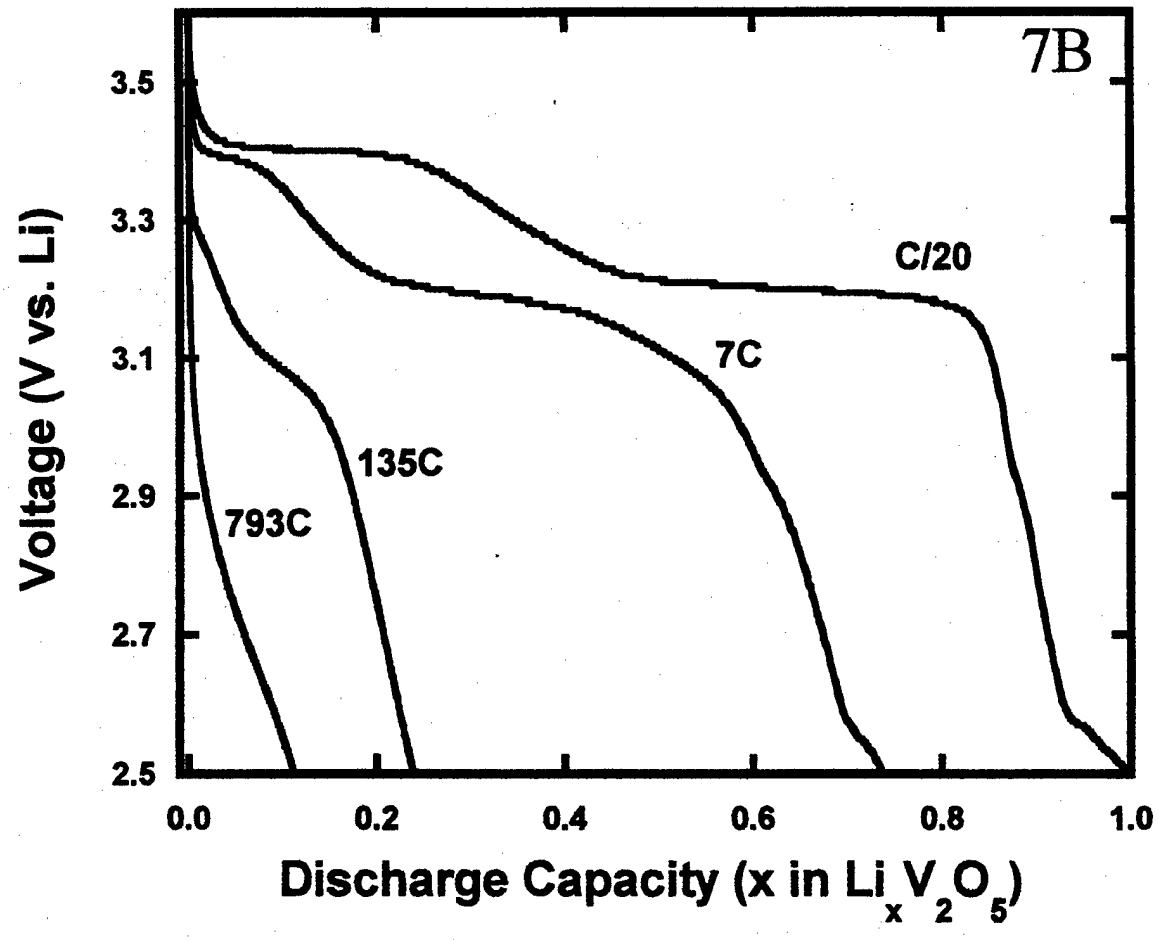
7B
Voltage (V vs. Li)
3.5
3.3
3.1
2.9
2.7
2.5
C/20
7C
135C
793C
0.0
0.2
0.4
0.6
0.8
1.0
Discharge Capacity (x in Li$_x$V$_2$O$_5$)

Figure 8

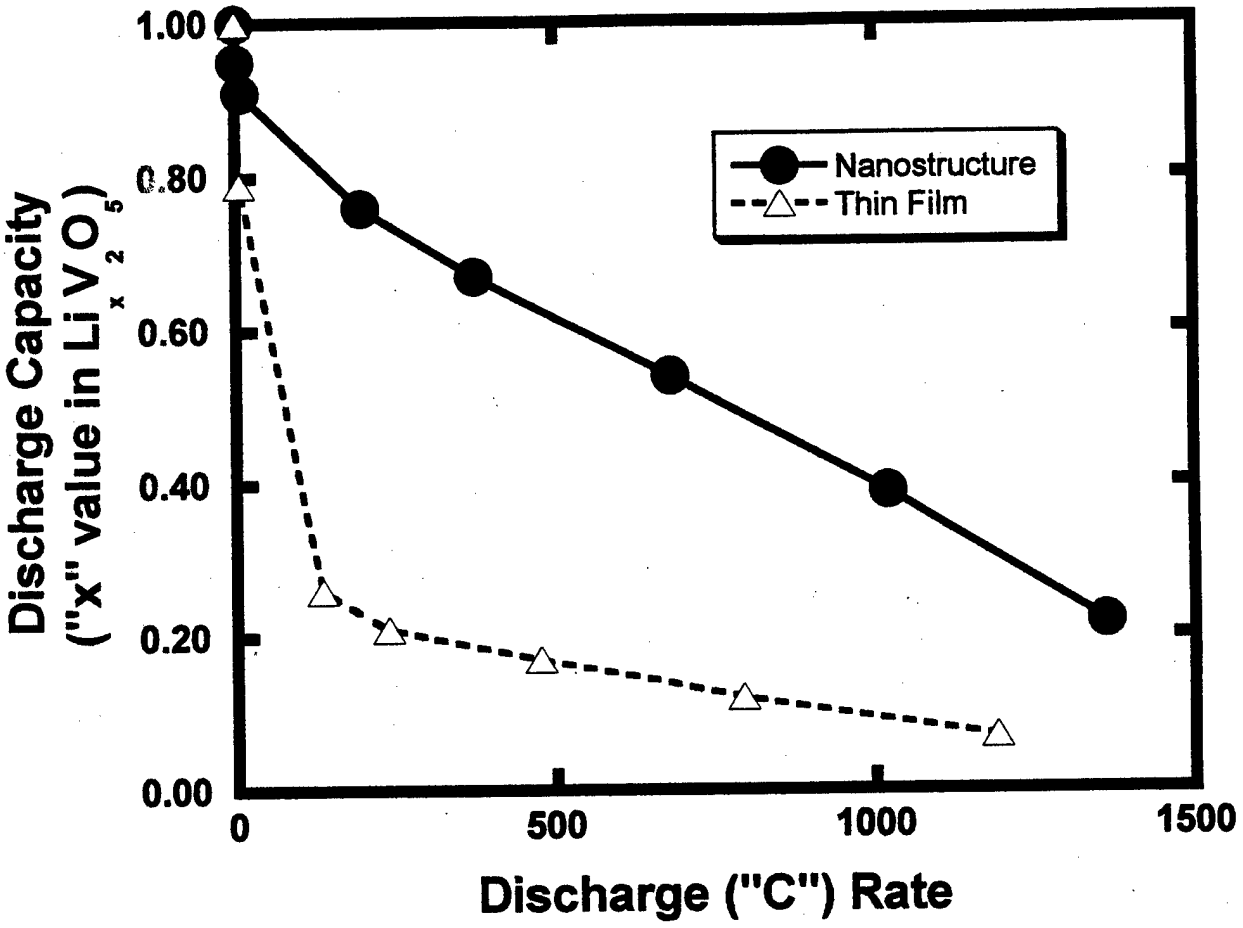
1.00
0.80
0.60
0.40
0.20
0.00
0
500
1000
1500
Discharge Capacity ("x" value in Li x V2O5)
Discharge ("C") Rate
Nanostructure
Thin Film